Heliyon 10 (2024) e37749

Contents lists available at ScienceDirect

Heliyon

journal homepage: www.cell.com/heliyon

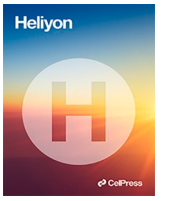

Research article

ALYREF enhances breast cancer progression by regulating EZH2

Su-Jin Jeong [a,b], Ji Hoon Oh [a,b,1], Je-Yoel Cho [a,b,*]

[a] Department of Biochemistry, College of Veterinary Medicine, Research Institute for Veterinary Science, and BK21 PLUS Program for Creative Veterinary Science Research and Research Institute for Veterinary Science, Seoul National University, Seoul, 08826, Republic of Korea
[b] Comparative Medicine Disease Research Center, Seoul National University, Seoul, 08826, Republic of Korea

ARTICLE INFO

Keywords:
Breast cancer
Epigenetics
Canine mammary tumor
ALYREF

ABSTRACT

Breast cancer is one of the most common malignant tumors in women worldwide. Similarly, Canine mammary tumors (CMTs) are mostly diagnosed as spontaneous diseases in female dogs. Many studies have suggested that CMTs serve as good models for human breast cancer. However, comparative approaches to histone modifications are still lacking. This study aimed to compare the canine mammary tumor Histone H3 lysine 4 trimethylation (H3K4me3) landscape with that in human breast cancer. Our H3K4me3 ChIP-seq data from CMTs revealed a significant enrichment of H3K4me3 in the ALYREF gene promoter in tumor tissues compared to normal tissues. Furthermore, our study and publicly available RNA-sequencing data revealed that *ALYREF* expression was elevated in malignant tissues and breast cancer cell lines, and its upregulation was associated with poor prognosis in humans. Depletion of ALYREF resulted in changes in cellular phenotypes, including increased proliferation and colony formation, as well as decreased apoptosis. *ALYREF* increased cell viability and anchorage-independent growth while decreasing apoptosis by regulating the mRNA expression and protein levels of enhancer of zeste 2 polycomb repressive complex 2 subunit (EZH2), which promotes hormone receptor-positive breast cancer and CMTs via epigenetic modifications. This suggests that *ALYREF* may function as a contributing factor to malignant transformation in both CMT and human breast cancer.

1. Introduction

Breast cancer is one of the most prevalent malignancies in women worldwide and is typically caused by a variety of genetic and environmental factors. Although age, family history, and genetic mutations (e.g., BRCA1 and BRCA2) are prominent non-modifiable risk factors, the disease etiology is multifaceted, necessitating a comprehensive understanding of effective clinical management [1]. The classification of primary breast cancer subtypes depends on the simultaneous expression of key tumor markers, such as the estrogen receptor (ER), progesterone receptor (PR), and human epidermal growth factor 2-neu (HER2), which guide clinical interventions. Population-based investigations have identified HER2 overexpression in approximately 20 % of early-stage breast cancer cases. This overexpression is often associated with increased recurrence rate and mortality, independent of nodal staging [2]. ER, a nuclear protein that regulates specific gene expression, is prevalent in approximately 80 % of patients with breast cancer who are considered to have a good response to first-line endocrine therapy. However, primary (*de novo*) resistance may manifest in some

* Corresponding author. Department of Biochemistry, College of Veterinary Medicine Seoul National University, Gwanak-ro1, Gwanak-gu, Seoul, Republic of Korea.
E-mail address: jeycho@snu.ac.kr (J.-Y. Cho).
[1] Current address: Department of Biological Sciences, Keimyung University College of Natural Sciences, Daegu 42601, Republic of Korea.

https://doi.org/10.1016/j.heliyon.2024.e37749
Received 1 May 2024; Received in revised form 8 August 2024; Accepted 9 September 2024
Available online 16 September 2024

Abbreviations

BP	Biological processes
CC	Cellular compartment
ChIP	Chromatin immunoprecipitation
CMT	Canine mammary tumor
CNV	Copy number variation
DAVID	Database for Annotation, Visualization, and Integrated Discovery
DHR	Differentially histone-modified regions
DNMT	DNA methyltransferase
EZH2	Enhancer of Zeste 2 Polycomb Repressive Complex 2 Subunit
ER	Estrogen receptor
FACS	Fluorescence-activated cell sorting
FBS	Fetal bovine serum
FDR	False discovery rate
GBM	Glioblastoma
GEO	Gene Expression Omnibus
GO	Gene Ontology
HCC	Hepatocellular carcinoma
HER2	Human epidermal growth factor receptor 2
KEGG	Kyoto Encyclopedia of Genes and Genomes
MBC	Metastatic breast cancer
MEGS	Mammary Epithelial Growth Supplement
MF	Molecular function
PR	Progesterone receptor
PRC	Polycomb repressive complex
SD	Standard deviation
SRA	Sequence Read Archive
TCGA	The Cancer Genome Atlas
TNBC	Triple-negative breast cancer
TREX	Transcription export
TSG	Tumor suppressor gene
TSS	Transcription start site

patients with ER + metastatic breast cancer (MBC), while others, although initially responsive, may eventually develop secondary (acquired) resistance, leading to disease progression in many cases [3].

Animal models have emerged as invaluable tools for studying cancer pathogenesis and developing therapeutic interventions. Canine mammary gland tumors (CMTs) represent a particularly relevant model because of their spontaneous occurrence in female dogs, mirroring the hormonal etiology (ER, PR, HER-2, and Ki-67) and clinicopathological characteristics of human breast cancer. Furthermore, their subtype-enriched transcriptomic signatures closely resemble those of human breast cancer [4,5]. Our previous study showed a remarkable resemblance of the PIK3CA hotspot mutation between dogs and humans, with both species sharing the same hotspot A3140G (H1047R) mutation, occurring in approximately 30 % of cases [6]. Moreover, the average age of onset and risk factors for CMT are similar to those for human breast cancer [4]. Due to their high epidemiological and histological similarities, CMTs serve as excellent models for studying human breast cancer [7,8]. Consequently, various studies, including genetic and epigenetic approaches, have been performed on CMT for human and canine comparative oncology [6,9–12].

Epigenetic modifications, including DNA methylation, histone modification, and modification of noncoding RNA, play pivotal roles in gene regulation and have been implicated in tumorigenesis. Post-translational histone modifications, such as methylation, acetylation, and phosphorylation, govern multiple cellular processes involved in tumorigenesis and progression by regulating chromatin accessibility. Histone H3 lysine 4 trimethylation (H3K4me3) is a well-defined modification that regulates preinitiation complex formation and interactions with the TFIID complex, ultimately leading to active gene expression [13]. Nuclear staining of H3K4me3 has been demonstrated to correlate with positive estrogen receptor (ER) status, shorter breast cancer-specific survival, and shorter progression-free survival. Additionally, patients with high nuclear H3K4me3 staining exhibit decreased overall survival [14]. Modification of histone H3 lysine 27 trimethylation (H3K27me3) is mediated by the enhancer of zeste homolog 2 (EZH2), a subunit of the polycomb repressive complex (PRCs), and is responsible for the repressed expression of genes. EZH2 expression is elevated in human breast cancer patients compared to that in normal or hyperplastic patients, correlating with aggressiveness and poor clinical outcomes. Moreover, EZH2 promotes anchorage-independent colony growth and invasion abilities in the breast epithelial cell line H16N2 as well as the proliferation of mouse embryonic fibroblasts [15].

ALYREF, an RNA-binding protein, plays a crucial role in transcriptional regulation and mRNA export, facilitating the nuclear-to-cytoplasmic export of mRNA, which is a pivotal step in gene transcription and mRNA processing. As a component of the transcription

export (TREX) protein complex, ALYREF binds to mature mRNA, facilitating its transfer to the cytoplasm [16]. ALYREF has been reported to be frequently amplified in various human cancers, its expression is dysregulated in cancers such as hepatocellular carcinoma (HCC) [17], neuroblastoma [18], glioblastoma [19], and triple-negative breast cancer (TNBC) [20]. In TNBC, upregulated *ALYREF* leads to enhanced *NEAT1* lncRNA expression and stabilization of CPSF6, which selectively regulates the post-transcriptional activity of NEAT1 [20]. ALYREF participates in diverse cellular processes, including cell proliferation, apoptosis, and migration, and exhibits varied responses depending on the cellular environment in multiple cancers, including TNBC. However, the precise function of ALYREF in non-TNBC cells remains unclear.

Here, we used chromatin immunoprecipitation sequencing (ChIP-seq) to investigate the global landscape of H3K4me3 in CMTs and identified increased *ALYREF* expression. Moreover, depletion of *ALYREF* induced apoptosis and decreased cell viability in both CMTs and human breast cancer cell lines, suggesting that *ALYREF* may play a tumor-promoting role.

2. Material and methods

2.1. Clinical samples

This study was reviewed and approved by the Seoul National University Institutional Review Board/Institutional Animal Care and Use Committee (IACUC SNU-170602-1, approval July 26, 2016), and all methods were performed in accordance with the relevant guidelines and regulations. For the ChIP-seq discovery phase, three pairs of specimens consisting of CMTs and adjacent normal tissues were collected from the dogs. To establish the primary cell line, one pair of specimens consisting of CMT and adjacent normal tissue were collected from dogs.

2.2. Canine mammary gland tumor (CMT) primary cell line establishment

The primary CMT cell line was established directly from digested CMT tissues obtained from the Veterinary Medical Teaching Hospital of Seoul National University using TrypLE Express solution containing the Rho kinase inhibitor Y-27632, DNase I, and Collagenase/Dispase. The digested cells were filtered and equilibrated in PBS containing 1X Mammary Epithelial Growth Supplement (MEGS). Primary cells were first cultured in advanced DMEM/F12 supplemented with 2 mM L-glutamine, penicillin (100 U/mL)–streptomycin (100 μg/mL), and 1X MEGS. Subsequent cell cultures were grown in DMEM with the same supplementation as mentioned above, except without additional L-glutamine and replacing MEGS with 10 % fetal bovine serum (FBS). All cells were grown in a humidified incubator at 37 °C with 5 % CO_2 and were tested regularly for mycoplasma contamination.

2.3. Cell culture

Human breast cancer cell lines and breast epithelial cell line MCF-10A were obtained from the Korean Cell Line Bank and cultured as previously reported [21]. Briefly, normal epithelial MCF-10A cells were cultured in MEBM Basal Medium (CC-3151; Lonza, Basel, Switzerland) or MEGM supplemented medium (CC4136; Lonza, Basel, Switzerland). SKBR3 cells were cultured in RPMI 1640 medium supplemented with L-glutamine (SH30027.01, Hyclone, UT, USA). MCF-7 cells were cultured in DMEM/high glucose supplemented with L-glutamine and sodium pyruvate (SH30243.01; Hyclone, UT, USA). CHMp canine mammary gland adenocarcinoma cell line was purchased from N. Sasaki lab [22] and grown in RPMI 1640 medium (HyClone, SH30027) containing 10 % FBS; Gibco 1600044) and 50 μg/mL gentamicin (Sigma–Aldrich, G1272). All cell lines were cultured at 37 °C in a 5 % CO_2 atmosphere. All cells were cultured in a humid incubator at 37 °C with 5 % CO_2, and their mycoplasma contamination was verified to be absent.

2.4. Expression and human ChIP-seq data set

Online datasets were retrieved from Gene Expression Omnibus (GEO, https://www.ncbi.nlm.nih.gov/geo/) and The Cancer Genome Atlas (TCGA, https://portal.gdc.cancer.gov/). This study utilized three public cohorts, GSE65194 and GSE119810, which encompass microarray expression profiles of normal and cancerous human breast and canine mammary tissues, respectively. Additionally, GSE85158 provided the H3K4me3 ChIP-sequencing data for human breast cancer cell lines. Student's t-tests were used to detect significant differences between two or more groups.

2.5. siRNA transfection

A total of 30 pmol each of ALYREF siRNA (Genolution, Seoul, South Korea) and SN-1012 (Bioneer, Daejeon, Republic of Korea) as negative controls were transfected with Lipofectamine RNAiMAX transfection reagent (Thermo Fisher Scientific, Waltham, MA, USA) according to the manufacturer's instructions. The cells were harvested 48 and 72 h after incubation for further analysis. The siRNA sequences are listed in Supplementary Table 1.

2.6. RNA extraction and quantitative RT-PCR

RNA extraction and quantitative RT-qPCR (qRT-PCR) were performed as previously reported [21]. Briefly, total RNAs were extracted using the TRIzol reagent (Thermo Fisher Scientific, Waltham, MA, USA) according to the manufacturer's instructions. Total

RNA (2 μg) was reverse transcribed into cDNA using the CellScript All-in-One 5 × First Strand cDNA Synthesis Master Mix (CellSafe, Yong-In, Republic of Korea) according to the manufacturer's instructions. The primers used for RT-qPCR are listed in Supplementary Table 1. The samples were run in triplicate and the expression of each target gene mRNA level was analyzed using the 2-ΔΔCT method and normalized to GAPDH expression in humans and dogs.

2.7. Gene ontology (GO) and Kyoto Encyclopedia of Genes and Genomes (KEGG) pathway analysis

GO and KEGG pathway enrichment analyses were performed using Database for Annotation, Visualization, and Integrated Discovery (DAVID) bioinformatics resources to predict the gene function of identified differentially histone-modified genes. The promoter region was defined as 2 kb upstream and downstream of the TSS.

2.8. Cell growth assay

Cell viability was determined using a Cell Counting Kit-8 (CCK-8; Dojindo, Tokyo, Japan) as previously described [23]. Briefly, cells were seeded into 96-well plates at 5000 cells for CHMp and 7500 cells (MCF7 and SKBR3) per well. A volume of 10 μL of CCK-8 reagent was added to each well. Plates were incubated for 3 h at 37 °C, and the absorbance value (OD) of each well was measured at 450 nm using a spectrophotometer (Epoch Microplate spectrophotometer, BioTek Instruments, Winooski, VT, USA) according to the manufacturer's instructions.

2.9. Cell migration assay

Cell migration was assessed as previously described [24]. The assay was performed using SPL Transwell inserts (#37224; SPL Life Sciences, Seoul, Korea) in 24-well plates. For all cells, approximately 5 × 104 cells in 200 μL of DMEM/high glucose medium (Hyclone, Logan, UT, USA) supplemented with 10 % US origin FBS (Hyclone, Logan, UT, USA) were placed in the chamber, and 500 μL of the same medium was added in the chamber. The plates were incubated at 37 °C in 5 % CO_2. After washing, cells were fixed and stained with crystal violet. Cells were counted under a microscope using ToupView software.

2.10. Colony formation assay

Five hundred cells were seeded 24 h after transfection in a 6-well plate with the appropriate media. After incubating the cells for 10–14 days at 37 °C in 5 % CO_2, they were fixed and stained with 2.5 % crystal violet and the number of colonies was counted.

2.11. Genome-wide ChIP-seq and ChIP-PCR

ChIP assays were performed on canine mammary tissue and human breast cancer cell lines to evaluate H3K4me3 (Abcam, ab8580, USA) and H3K27me3 (Abcam, ab6002, USA) enrichment, according to a previous study. Briefly, the samples were fixed with 1 % formaldehyde in a rocker at room temperature for 10 min to cross-link histones to DNA, and the reaction was stopped by adding glycine to a final concentration of 125 mM. The DNA was then sheared by sonication to generate 300–600 bp DNA fragments. Immunoprecipitation was performed with the H3K4me3 antibody at a concentration of 5 μg per 25 μg chromatin, and the same amount of normal IgG (AC-005, Abclonal, China) was used as control. The precipitated DNA was detected by RT-PCR using specific primers (Supplementary Table S1). Across all generated in-house ChIP-seq datasets, the CanFam3.1 genome was used as a reference genome assembly. The ChIP-seq data were processed as in our previous study [25].

2.12. Protein extraction and western blot analysis

Protein extraction and western blotting were performed as described previously [21]. Immunoblotting was performed and antibodies specific for ALYREF (1:1000, A4298, Abclonal, China), BAX (1:500, a12009, Abclonal, China), and B-Actin (1:1000, sc-47778, Santa Cruz Biotechnology, Santa Cruz, USA). Images were quantified using ImageJ and relative optical densities were calculated by adjusting to B-actin loading control.

2.13. Statistical analysis

All statistical analyses were performed using Prism software (version 8.0.1; GraphPad Software, La Jolla, CA, USA). For statistical significance between the two groups, the Student's t-test was performed. Data are expressed as mean ± standard deviation (SD). n values indicate the number of individual experiments conducted. Significant differences are indicated by different letters in figure legends.

3. Result

3.1. Genome-wide analysis of H3K4me3

To determine the differences in H3K4me3 active histone-marked genes between normal and cancerous tissues, we performed ChIP-seq using the three CMTs and matched normal mammary gland tissues obtained from individuals during surgery (Fig. 1a and Table 1). DNA fragments pulled down by ChIP-grade antibodies against H3K4me3 were aligned using the CamFam3.1 database. The differentially histone-marked gene was defined as regions exhibiting a 1.5-fold higher or lower change in H3K4me3 binding compared to adjacent normal tissues, with a false discovery rate (FDR) adjusted to a p-value of $\leq$0.05. Sequence statistics are summarized in Supplementary Table 2.

A total of 3943 H3K4me3 histone-marked regions were identified in the tissue comparison, with 1858 identified as high and 2085 identified as low in the tumor. To better understand the H3K4me3 ChIP landscape of CMT, all histone-marked regions were separated according to their genomic distribution in both gene or intergenic regions. Promoters were defined as those located 2 kb upstream and/or downstream of the transcription start site (TSS). A total of 434 (11 %) regions were annotated as promoter regions, 361 (9.1 %) regions were annotated as exon, 1616 (42 %) regions were annotated as intron, and 1435 (36.3 %) regions were annotated as

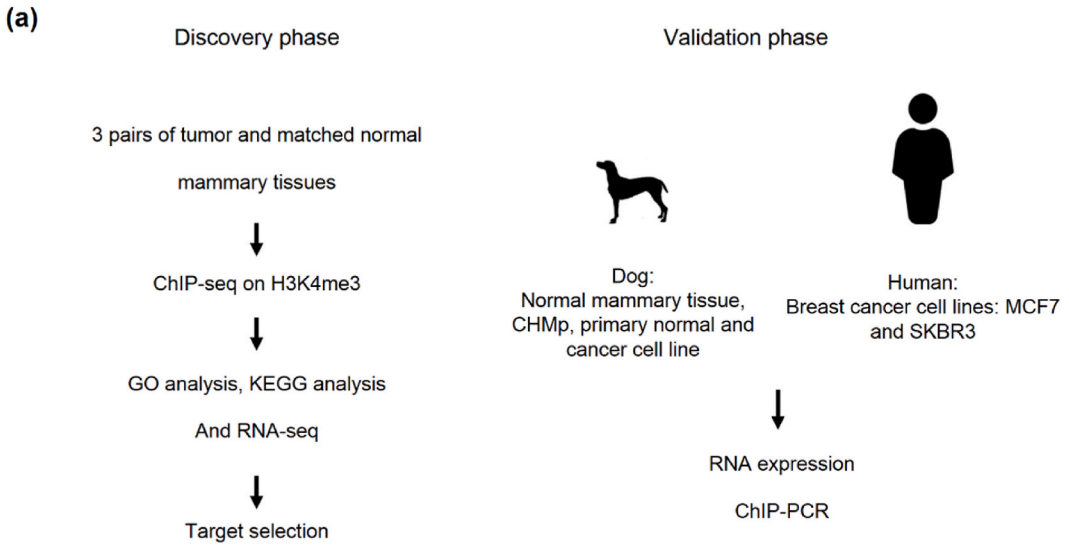

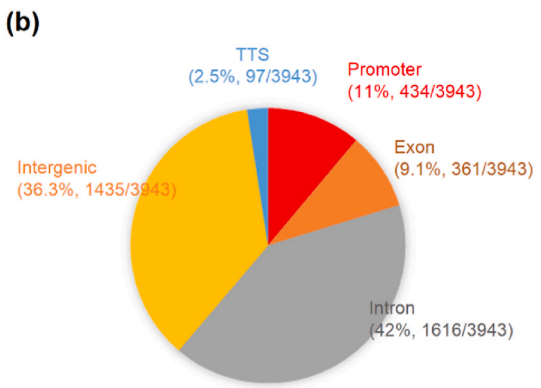

Total	Promoter	Exons	Introns	Intergenic	TTS
3943	434	361	1616	1435	97

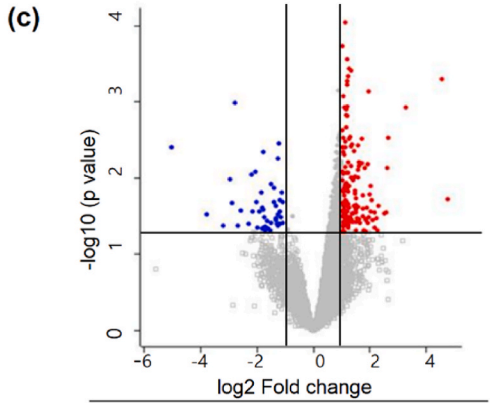

	promoter	1.5↑	1.5↓
H3K4me3	434	383	51

Fig. 1. Scheme of research flow and statical summary of histone-marked regions.
(a) Scheme of this study from discovery to validation. (b) Genomic distribution of differentially histone-modified regions (DHRs) defined by a 1.5-fold difference. False discovery rate (FDR) is adjusted q-value $\leq$0.05 in CMT tissues. (c) Volcano plots of all DHRs in the promoter region. The colors indicate significant methylation: hyper (red) and hypo (blue). The x-axis represents log2 fold change and the y-axis represents −log10 q-value.

Table 1
Patients' information.

Patient ID	Sex	Age	Breed	Diagnosis
CCRCD0001	F	10y	Great Pyrenees	Mammary Gland complex Carcinoma
CCRCD0095	FS	11y	Maltese	Mammary Gland adenocarcinoma
CCRCD0125	FS	16y	Schnauzer	Mammary Gland tubular carcinoma
CCRCD1111	FS	7y	Maltese	Mammary Gland complex Carcinoma

intergenic regions (Fig. 1b). The volcano plot in Fig. 1c shows the genes annotated in the promoter region. A significantly higher number of genes were enriched for H3K4me3 marks (Fig. 1c).

3.2. Gene ontology (GO) and KEGG pathway analysis of the gene set differentially marked by H3K4me3

To investigate the H3K4me3-marked genes that were aberrantly enriched in tumors, GO functional analysis was performed using

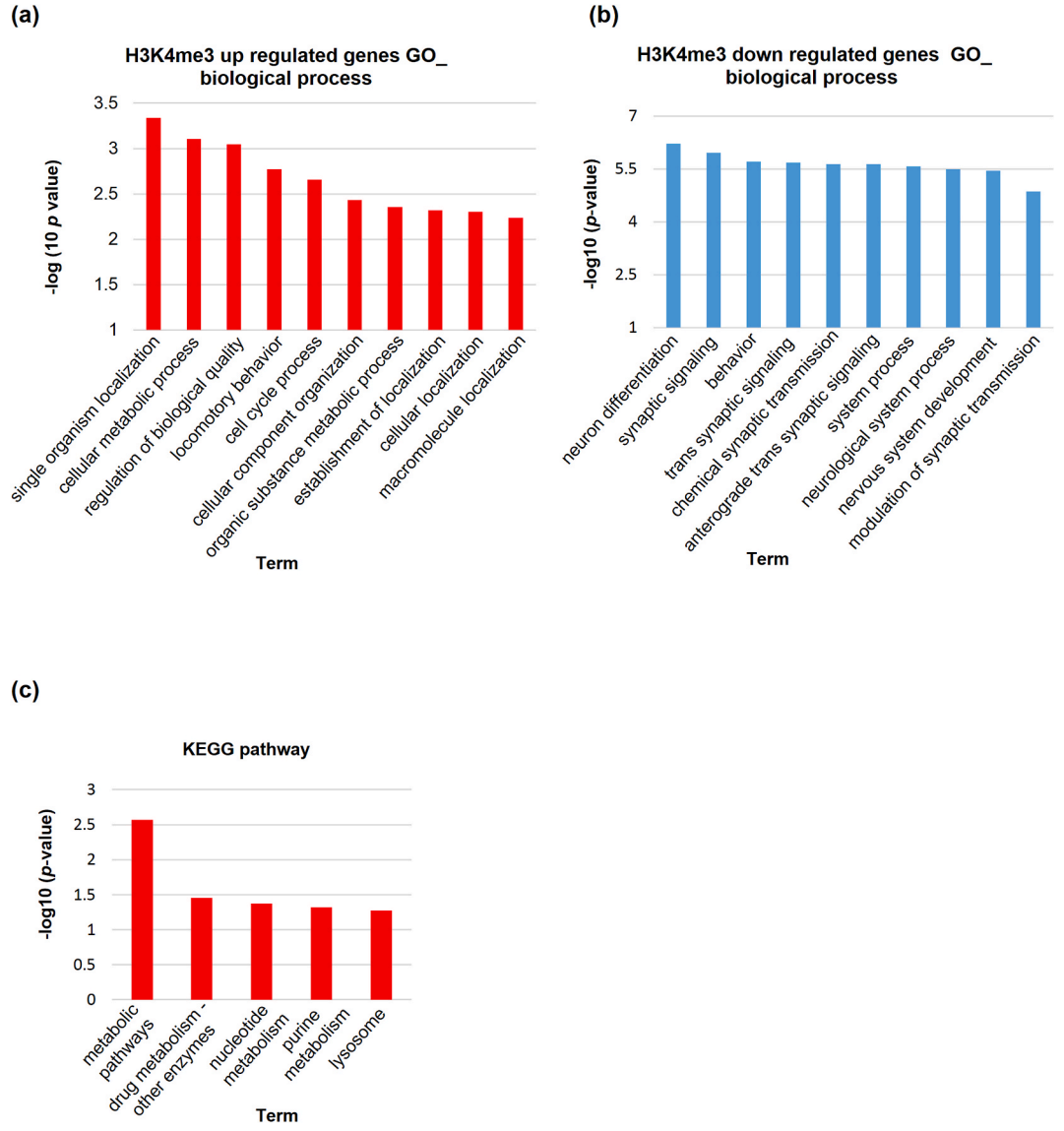

Fig. 2. Gene ontology (GO) and KEGG pathway analysis.
(a–c) Enrichment analysis of gene ontology (GO) and KEGG pathway using differentially histone-marked genes in CMT. The top 10 significant GO_BP terms and the top 5 KEGG terms are depicted. (a) Gene Ontology (GO) analysis of genes exhibiting a 1.5-fold increase and (b) decrease in H3K4me3, and (c) KEGG analysis of genes with increased H3K4me3.

DAVID. The results revealed diverse cancer-associated terms. A total of 329 genes with a more than 1.5-fold highly enriched H3K4me3 marks in tumors compared with adjacent normal tissues were categorized into 41 subcategories in biological processes (BP), 23 subcategories in molecular function (MF), and 28 subcategories in the cellular compartment (CC) (data not shown). The top 10 GO terms in the BP categories are listed according to the *p*-value in Fig. 2a and b. We observed processes associated with carcinogenesis, such as cell cycle regulation (GO:0051726) organic substance metabolic processes (GO:0071704), and upregulated GO. These GO terms were upregulated in human breast cancer [26,27]. The terms of H3K4me3 downregulated genes were highly enriched in the nervous system (GO:007399)-related terms (Fig. 2b).

KEGG pathway analysis revealed that genes with high levels of H3K4me3 were predominantly enriched in metabolism-related pathways, including those for drugs, nucleotides, and purines. Among the 39 genes associated with these pathways, we identified several well-known breast cancer-related genes, including *SQLE*, *SRD5A1*, and *UAP1*. Analysis of human cohorts and Kaplan–Meier (KM) plots indicated that the upregulation of *SQLE*, *SRD5A1*, and *UAP1* was associated with poor prognosis and reduced survival in patients with breast cancer [28–30]. To validate the impact of H3K4me3 histone modifications on metabolism-related gene expression in cancer cells, their expression levels were assessed. The expression of all three genes was upregulated in CMT and human breast cancer cell lines compared to normal cells (Supplementary Figs. 1a–c). A web-based Kaplan–Meier plotter (https://kmplot.com/analysis/index.php?p=service) was used to draw the KM plots. The KM plots revealed that *SQLE*, *SRD5A1*, and *UAP11* upregulation led to poor prognosis and survival in patients with breast cancer.

In summary, we found that the upregulation of metabolism-related genes *SRD5A1*, *UAP1*, and *SQLE* by higher H3K4me3 marks in CMT and their higher expression levels were also demonstrated in both canine and human breast cancers (Supplementary Figs. 1a–c). Our findings suggest that histone modifications could potentially influence expression changes in genes associated with metabolism.

3.3. H3K4me3 modification of ALYREF promoter changes in canine mammary tumor

The top 20 genes in the H3K4me3 highly enriched group are listed in Table 2 based on their respective *p*-values. The KM plot (Supplementary Figs. 2a–h) revealed that recurrence-free survival (RFS) was significantly less favorable in patients with high *KIAA0895, SQLE, TONSL, COMMD5, DOLK, CCDC137, ALYREF*, and *P3H4 (SC65)* expression (Table 2 and Supplementary Figs. 2a–h). We conducted a literature search on *KIAA0895, SQLE* [28,31,32], *TONSL* [33,34], *COMMD5* [35,36], *DOLK, CCDC137* [37], *ALYREF* [17,19,20], and *P3H4(SC65)* [38,39] to identify gene signatures associated with breast cancer. Despite having the lowest *p*-value in the KM plot, we found that research on ALYREF in hormone receptor-positive breast cancer is lacking, except for TNBC [20]. *ALYREF*, implicated in mRNA expression and RNA splicing, has shown elevated expression in numerous cancer patients based on data from TCGA. Despite the relevance of *ALYREF* in various types of cancer, including its potential involvement in tumorigenesis, its role in hormone receptor-positive breast cancer remains unclear. Consequently, we conducted subsequent experiments utilizing ALYREF.

We hypothesized that *ALYREF* might be involved in the malignant transformation of breast cancer in dogs and humans. To test this hypothesis, we initially conducted a comparative analysis of the *ALYREF* gene structure in humans, dogs, and mice (Fig. 3a). DNA sequence homology and the NCBI database were used to construct a phylogenetic tree based on the amino acid sequences of *ALYREF* isolated from humans, canines, and mice (Fig. 3b and c). The genetic architectures of humans and dogs exhibited a greater degree of similarity than those of humans and mice. Moreover, DNA and amino acid sequences displayed a high level of homology between humans and dogs.

To clarify the relationship between histone modification and *ALYREF* expression, we analyzed RNA-seq data from CMT tissues, a pair of primary CMT cell lines, and a CHMp cell line using RT-qPCR. Based on the ChIP-seq data obtained in our lab, we observed peaks

Table 2
The top 20 genes according to ChIP-seq p-value.

Gene	ChIP-seq p-value	Poor RFS	KM plot p-value	Breast cancer	Other cancers
KIAA0895	9.08E-05	high	0.01		
SQLE	0.00019	high	8.6E-16	[28,32]	[31]
SPHK1	0.00027	ns	0.9262		
CELSR3	0.00037	ns	0.058		
ABR	0.00039	low	4.20E-10		
TONSL	0.00046	high	0.0039	[34]	[33]
NDUFAF8	0.00053	ns	0.13		
COMMD5	0.0031	high	0.0031	[36]	[35]
DOLK	0.0007	high	0.009	[40]	
NKX2-4	0.00083	Not available			
CCDC137	0.0037	high	0.0037	[37]	[37]
TEPSIN	0.00117	ns	0.13		
ALYREF	0.00149	high	1.70E-16	[20]	[16–18]
SPAG6	0.00155	low	2.30E-10		
C15H1orf122	0.00213	Not available			
P3H4	0.00236	high	0.009	[39]	[38]
INSIG1	0.0025	ns	0.055		
AK8	0.0029	low	0.0014		
COMMD8	0.00293	low	0.41		
SPTAN1	0.00296	low	2.20E-09		

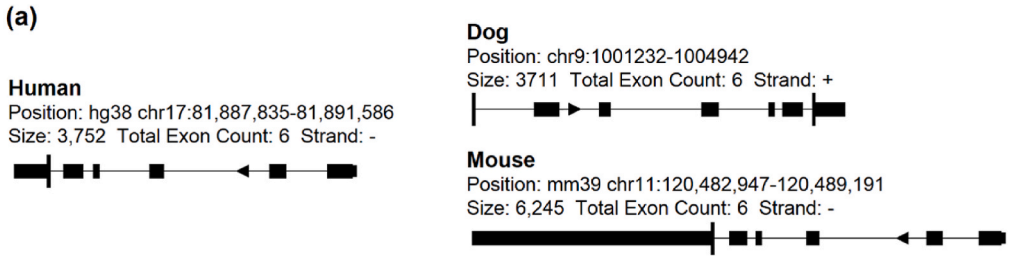

(b)

	Similarity with human nucleotide	
	Query	Sequence homology
Dog	78%	81.47%
Mouse	63%	79.31%

(c)

	Similarity with human amino acid	
	Query	Sequence homology
Dog	100%	91%
Mouse	100%	89%

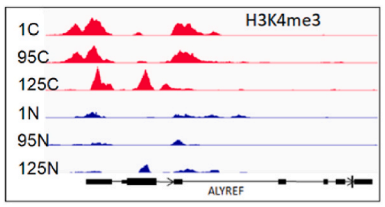

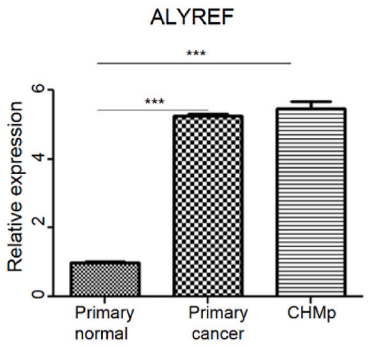

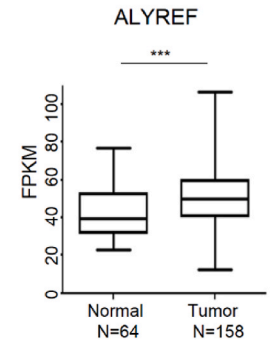

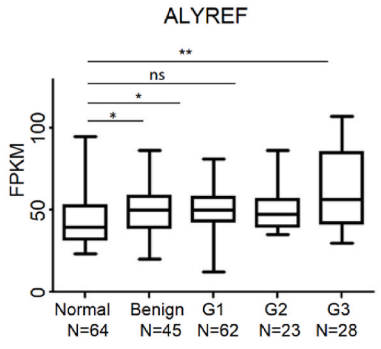

Fig. 3. Comparison of ALYREF orthologous regions of the human, dog, and mouse genome and analysis of *ALYREF* gene expression in cancer and normal specimens from Gene Expression Omnibus (GEO) dataset.

(a) Schematic structures showing *ALYREF* genes of humans, dogs, and mice. (b) Query cover and homology of *ALYREF* genes in DNA sequences between human and dog, and between human and mouse, respectively. (c) Query cover and homology in amino acid sequence between human and dog, and between human and mouse, respectively. (d) IGV browser screenshots of H3K4me3 ChIP-seq analysis in 3 pairs of CMTs. Each peak of H3K4me3 reveals respective specimens. The top three tracks reveal H3K4me3 signals in cancer tissues, others show signals in normal tissues. (e) Quantification of *ALYREF* expression in CHMp, a pair of primary cell lines. *ALYREF* expression was higher in CMT cell lines compared with normal cell lines. Data are presented as mean ± SEM (n = 3). The Student's t-test was used to analyze the data, and statistical analysis was performed. $*p < 0.05$, $**p < 0.01$, $***p < 0.001$. (f–g) Quantification of *ALYREF* expression in CMT tissues (n = 158) and healthy controls (n = 64) using the GEO dataset (GSE119810). (f) Expression of the *ALYREF* gene was relatively higher in CMT tissues compared with normal tissues. (g) Expression of the *ALYREF* gene was relatively upregulated in CMT tissues based on tumor grade. The x-axis represents sample numbers and tumor grades, and the y-axis represents the FPKM value. (h) IGV browser screenshots depict H3K4me3 ChIP-seq peaks in breast cancer cell lines, utilizing the GEO dataset (GSE85185). The top three tracks reveal SKBR, MCF7, and MDA-MB-231 (red), and the bottom track signals represent a normal cell line, MCF 10A (blue). (i) Quantification of *ALYREF* expression in breast cancer cell lines. *ALYREF* expression was higher in breast cancer cell lines compared with

normal cell lines. Data are presented as mean ± SEM (n = 3). The Student's t-test was used to analyze the data, and statistical analysis was performed. *$p < 0.05$, **$p < 0.01$, ***$p < 0.001$. (j–k) Quantification of *ALYREF* expression in human breast cancer tissues (n = 115) and healthy control (n = 11) using the GEO dataset (GSE65194). (j) Expression of the *ALYREF* gene was relatively higher in human breast cancer tissues compared with normal tissues. (k) Expression of the *ALYREF* gene was relatively upregulated in breast cancer tissues based on tumor grade. The x-axis represents sample numbers and tumor subtypes, and the y-axis represents relative expression.

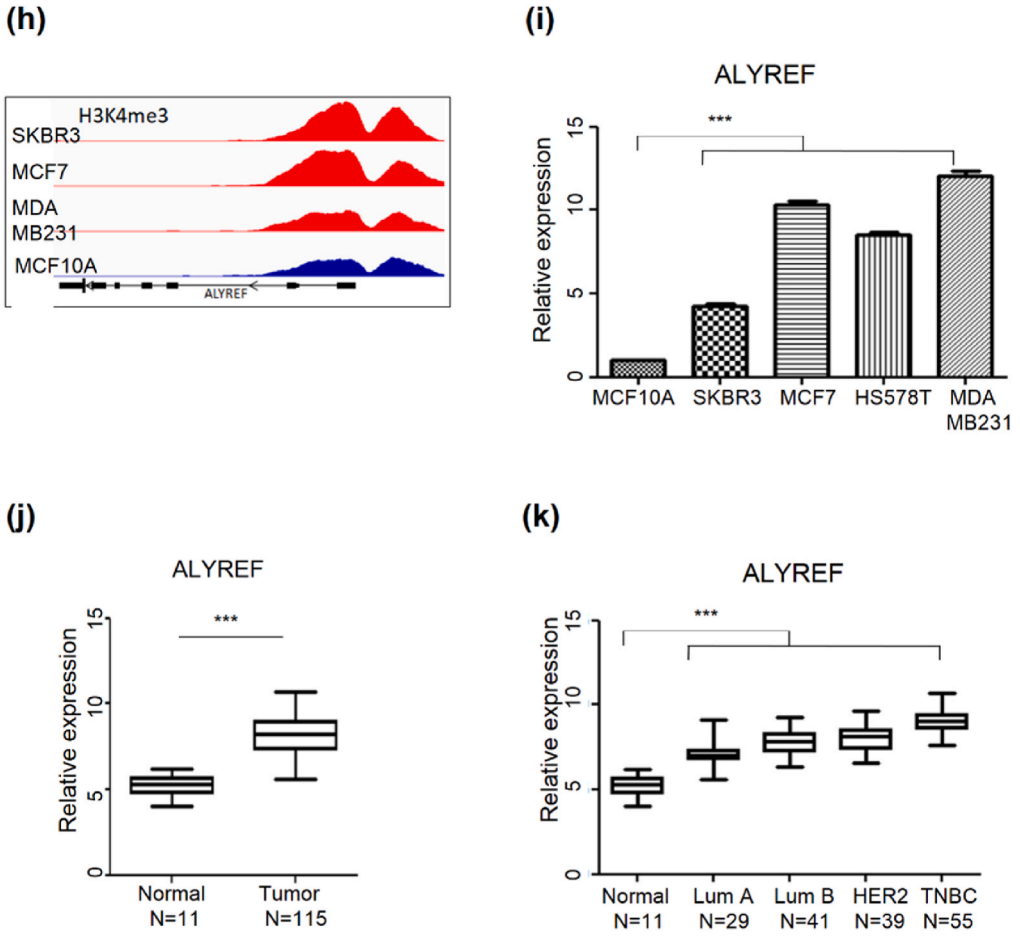

Fig. 3. (*continued*).

of H3K4me3 at chr9: 397, 497-398, 880, located 710bp upstream from the TSS of *ALYREF*. These peaks were highly enriched in a fraction of CMT tissues compared to those in normal tissues (Fig. 3d). Additionally, RNA expression levels were higher in primary cancer and CHMp cell lines than in primary normal cells (Fig. 3e). Our previous RNA-seq study performed in CMT tissues, had shown that *ALYREF* expression was higher in cancer tissues than in normal tissues. Moreover, as the tumor grade of the cancer tissue increased, *ALYREF* expression levels tended to increase (Fig. 3f and g). Similar to the findings in canines, a comparable pattern was observed in humans, wherein breast cancer cell lines (SKBR3 and MCF7) exhibited elevated levels of H3K4me3and *ALYREF* expression (Fig. 3h and i) compared to normal cell lines. Moreover, *ALYREF* expression was significantly higher in the cancer tissues than in the normal tissues (Fig. 3j). As the tumor grade increased in cancer tissues, there was a concurrent increase in *ALYREF* expression (Fig. 3k). The correlation between *ALYREF* expression and cancer grade indicates the involvement of *ALYREF* in the malignant transformation of non-TNBC breast cancers.

3.4. *ALYREF affects cell viability, colony formation and apoptosis*

To investigate the function of *ALYREF* in breast cancer cells, *ALYREF* was depleted in three independent cell lines: CHMp, SKBR3, and MCF7. The depletion efficiency of *ALYREF* in cell lines was estimated by RT-qPCR and Western blot analyses (Fig. 4a–e; since the ALYREF antibody did not guarantee cross-reactivity in dogs, Western blot data for canines are not presented). The CCK-8 assay revealed that cell viability was significantly reduced in all three *ALYREF*-depleted cell lines (Fig. 4f–h). To demonstrate tumor formation *in vitro*, we performed a colony formation assay. Fewer colonies were formed in *ALYREF*-depleted cell lines than in scrambled siRNA control cells (Fig. 4i–k), suggesting that *ALYREF* affects tumor cell proliferation and colony formation.

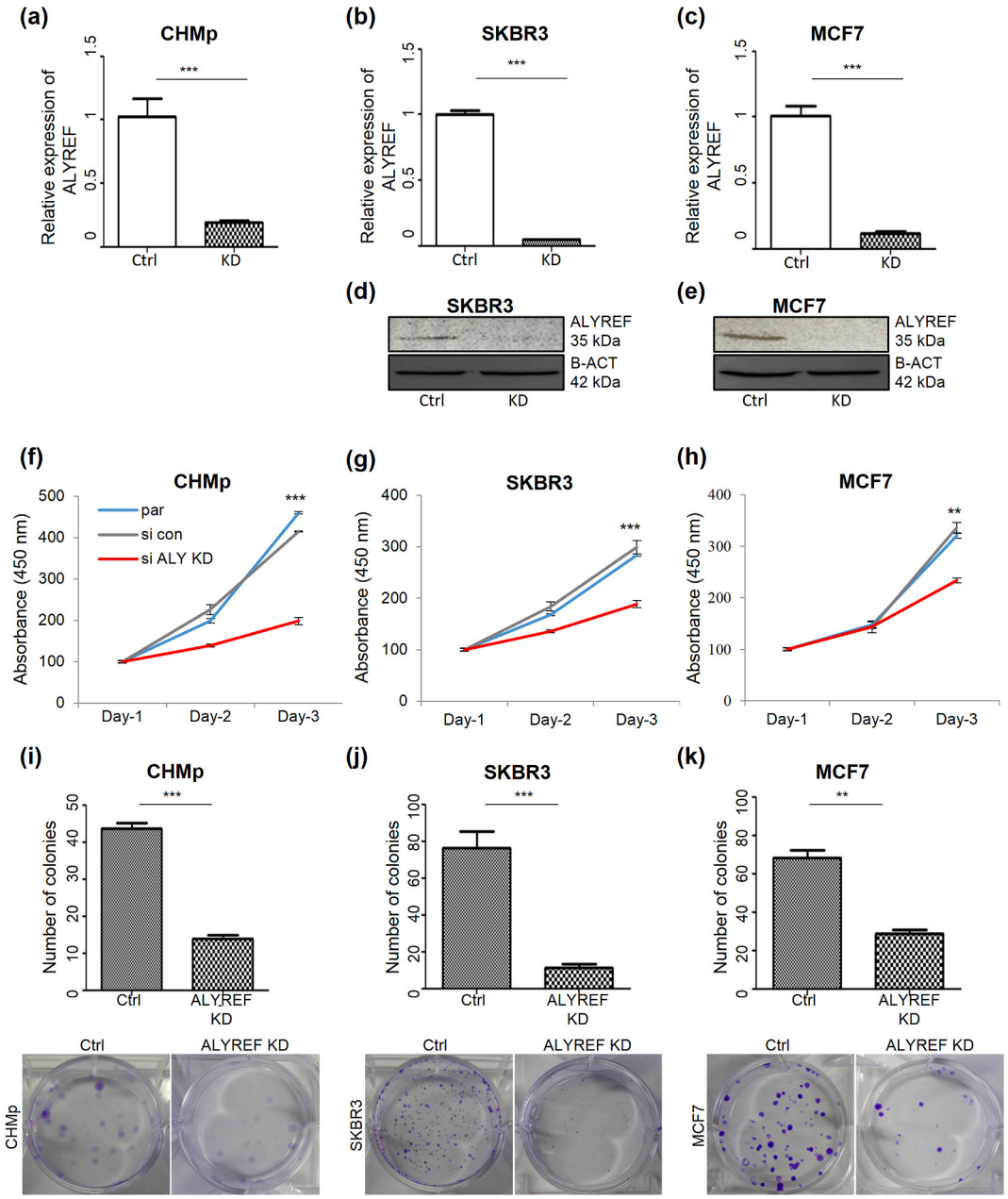

Fig. 4. Cellular consequences of loss of *ALYREF* function in CMT and human breast cancer cells.
(a–c) Quantification of depletion efficiency of *ALYREF* in CHMp and different breast cancer cell lines after treatment with specific siRNAs against *ALYREF* or control siRNA 72 h after transfection on mRNA level via RT-qPCR using *GAPDH* as a reference gene. n = 3, ±SD. ***$p < 0.001$. (d–e) Verification of siRNA-mediated depletion efficiency of *ALYREF* in (d) SKBR3 and (e) MCF7 cells on protein level analyzed by Western blot using β-Actin as loading control. (f–h) Cellular growth assay in breast cancer cells over 72 h under control conditions (control siRNA; gray, untreated parental control; blue) or after siRNA-mediated depletion of *ALYREF* (red). n = 3, ±SD. ***$p < 0.001$, **$p < 0.01$ (f) Depletion of *ALYREF* inhibited proliferation of the CMT cell line. Depletion of *ALYREF* inhibited the proliferation of (g) SKBR3 and (h) MCF7. (i–k) Colony formation assay in (i) CHMp, (j) SKBR3, and (k) MCF7. Below the bar graphs show representative stained colony formation figures with 3 wells each under control conditions or after siRNA-mediated *ALYREF* depletion. n = 3, ±SD. ***$p < 0.001$. (l–n) Flow-cytometry-based AnnexinV staining of the CMT cell line, SKBR3, and MCF7 72 h after silencing by control siRNA or siALYREF. Statistical significance between cells was assessed using Student's t-test. n = 3, ±SD. *$p < 0.05$, **$p < 0.01$, and ***$p < 0.001$.

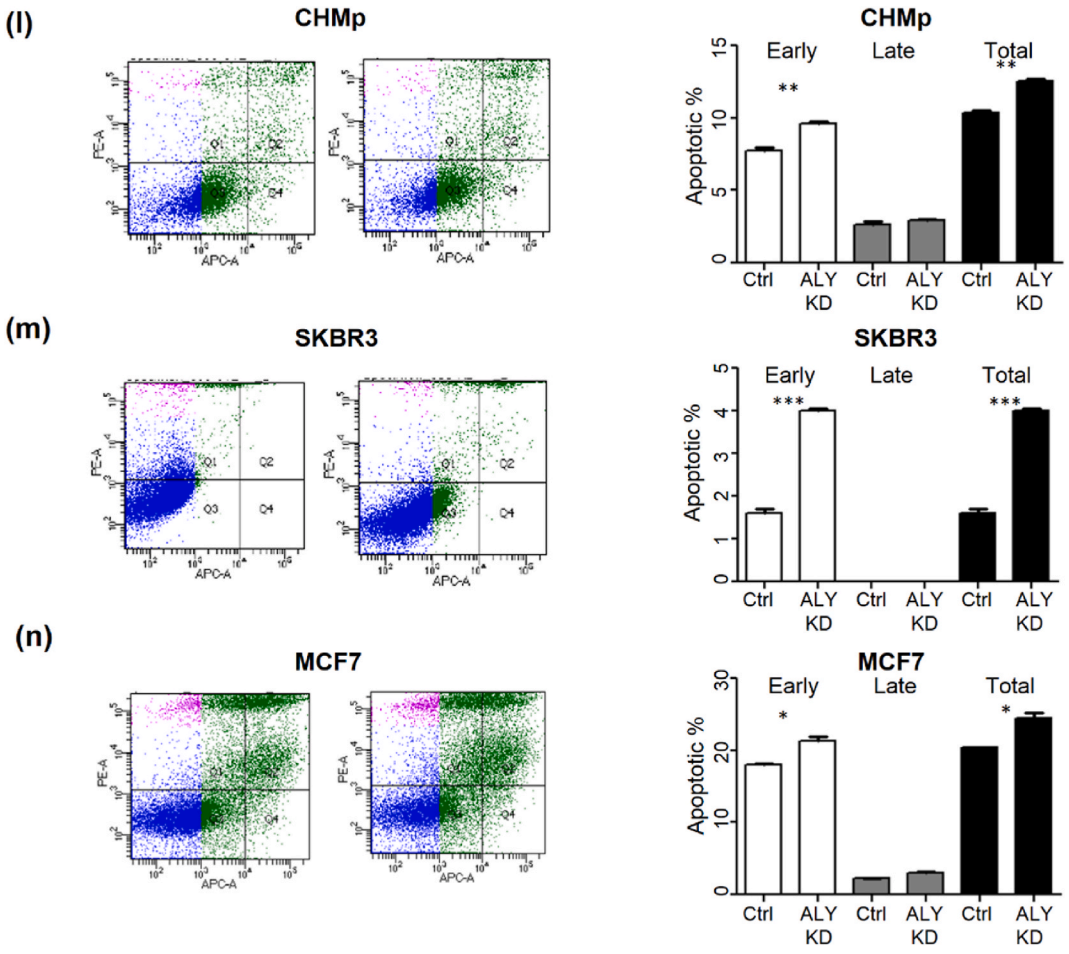

Fig. 4. (*continued*).

After identifying *ALYREF* as an important factor in tumor cell viability and colony formation, we investigated the effect of *ALYREF* depletion on the migration of breast cancer and CMT cell lines. Despite *ALYREF* depletion, there were no significant differences in tumor cell migration and cell cycle distribution compared to control cells (Supplementary Figs. 3a–f).

Annexin V-fluorescence-activated cell sorting (FACS) was performed to determine the role of *ALYREF* in apoptosis. *ALYREF* depletion increased apoptosis in all three breast cancer cell lines (Fig. 4l–n).

3.5. *ALYREF regulates breast cancer cell apoptosis through epigenetically suppressing BAX gene transcription*

To elucidate which apoptotic genes contributed to the increased apoptosis induced by *ALYREF* depletion, RT-qPCR was employed to examine changes in the expression of previously described pro- or anti-apoptosis-related genes, *BAX, BCL2, BI1*, and *MCL1*, following *ALYREF* depletion (Supplementary Figs. 4a and b) [41]. Among the apoptosis-related genes, *BAX* mRNA expression and protein levels were upregulated in *ALYREF*-depleted cells compared to those in control cells (Fig. 5a and b). BAX protein levels also substantially increased after *ALYREF* depletion (Fig. 5c and d). These findings suggested that *ALYREF* influences *BAX* transcription in human breast cancer cells. Next, we investigated the mechanisms underlying the regulation of *BAX* expression.

It has been reported that *ALYREF* can bind to the *EZH2* mRNA [16]. EZH2 is a well-known epigenetic modifier responsible for H3K27me3. *EZH2* expression levels were higher in patients with breast cancer than in healthy individuals (Fig. 5e). To investigate the effects of *ALYREF* on *EZH2* expression, we conducted an *EZH2* RT-qPCR analysis and a western blot assay, observing a decrease in *EZH2* mRNA and protein levels in the depleted cell lines (Fig. 5f and h). We hypothesized that there may be a chromatin mark for H3K27me3 at the *BAX* gene promoter locus that modulates transcriptional processes. Thus, we analyzed the H3K27me3 modification levels at the *BAX* promoter using ChIP-PCR in human breast cancer cell lines. H3K27me3 levels at the *BAX* promoter were higher in cancer cell lines than in normal cell lines (Fig. 5i). We also demonstrated that enrichment of H3K27me3 at the *BAX* promoter was reduced in *ALYREF*-depleted cells. (Fig. 5j and k).

Our results indicate that *ALYREF* is a novel factor involved in the tumorigenesis of human and canine breast cancer, partly through the regulation of the anti-apoptotic *BAX* gene via H3K27me3 epigenetic modulation.

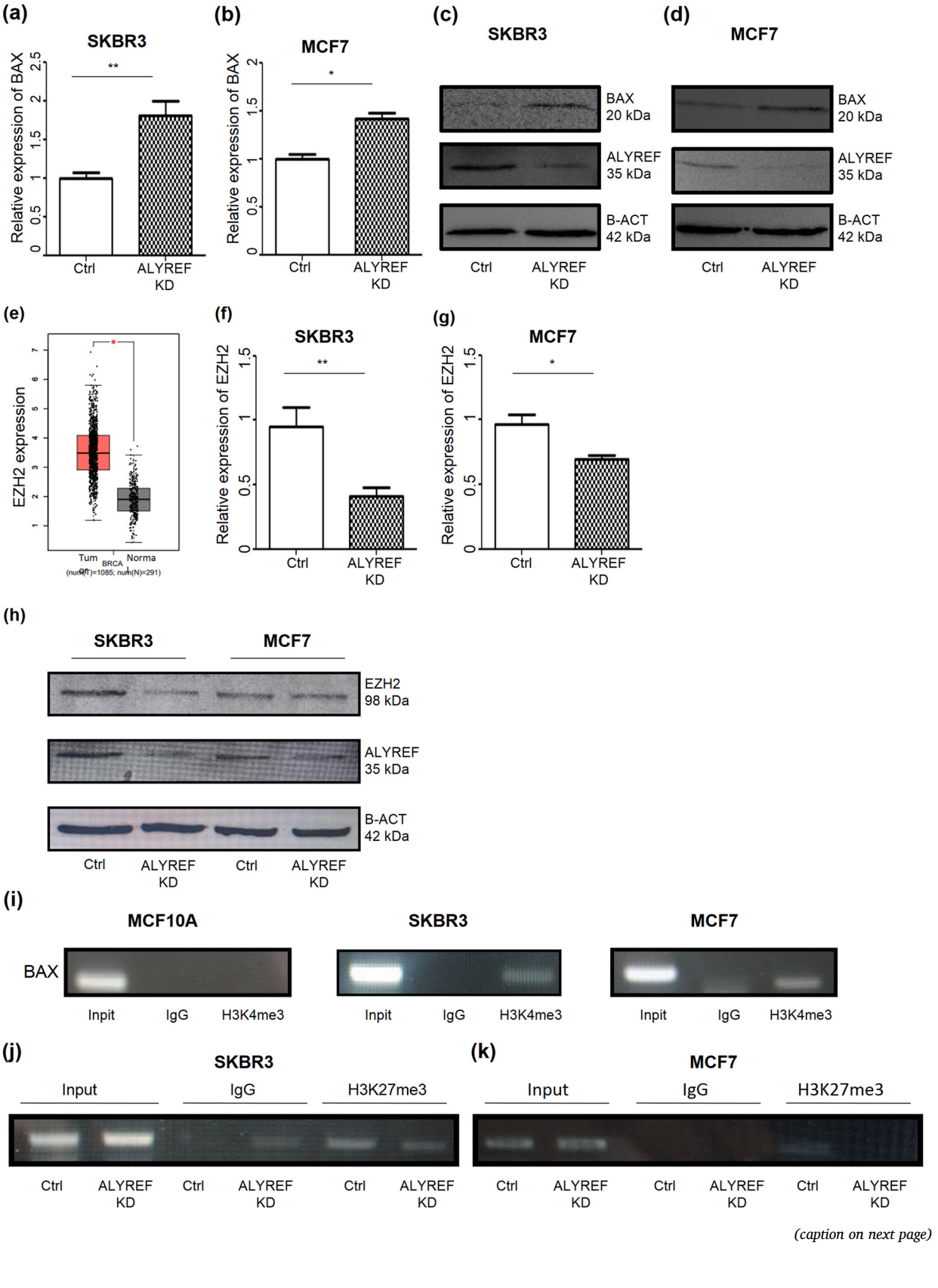

(caption on next page)

Fig. 5. *ALYREF* depletion induces apoptosis in breast cancers through an epigenetic mechanism.
(a–b) Quantification of *BAX* mRNA expression shows an increased *BAX* mRNA in *ALYREF*-depleted breast cancer cell lines. *BAX* mRNA expressions were measured in **(a)** SKBR3 and **(b)** MCF7 cell lines by RT-qPCR using GAPDH as a housekeeper in comparison to the control siRNA. n = 3, ±SD. **(c–d)** After *ALYREF* depletion, BAX protein levels increased in *ALYREF*-depleted **(c)** SKBR3 and **(d)** MCF7 cell lines. β -Actin was used as a loading control in the Western blot. **(e)** The expression profiles of *EZH2* genes in breast cancer. Data were derived from the publicly available GEPIA database. The box plot showed the increased EZH2 expression in tumor tissues (T, red box, n = 1085) compared to normal tissues (N, gray box, n = 291) **(f–g)** *EZH2* mRNA expressions were measured in **(f)** SKBR3 and **(g)** MCF7 cell lines by RT-qPCR using GAPDH as a housekeeper in comparison to the control siRNA. **(h)** Western blot analysis shows decreased EZH2 protein levels after depletion of *ALYREF* using β-Actin as loading control. **(i)** Chromatin immunoprecipitation in MCF10A, MCF7, and SKBR3 cell lines with an antibody against H3K27me3 or a negative control antibody (Mock IgG) and subsequent PCR using primers specific for BAX promoter regions. H3K27me3 levels on the *BAX* promoter were higher in SKBR3 and MCF7 cell lines compared to normal MCF10A cell lines. **(j–k)** Chromatin immunoprecipitation in **(j)** SKBR3 and **(k)** MCF7 control and after depletion of cell lines with an antibody against H3K27me3 or a negative control antibody (Mock IgG) and subsequent PCR using primers specific for *BAX* promoter regions. H3K27me3 levels on *BAX* promoter were decreased after depletion of *ALYREF* in both MCF7 and SKBR3 cell lines.

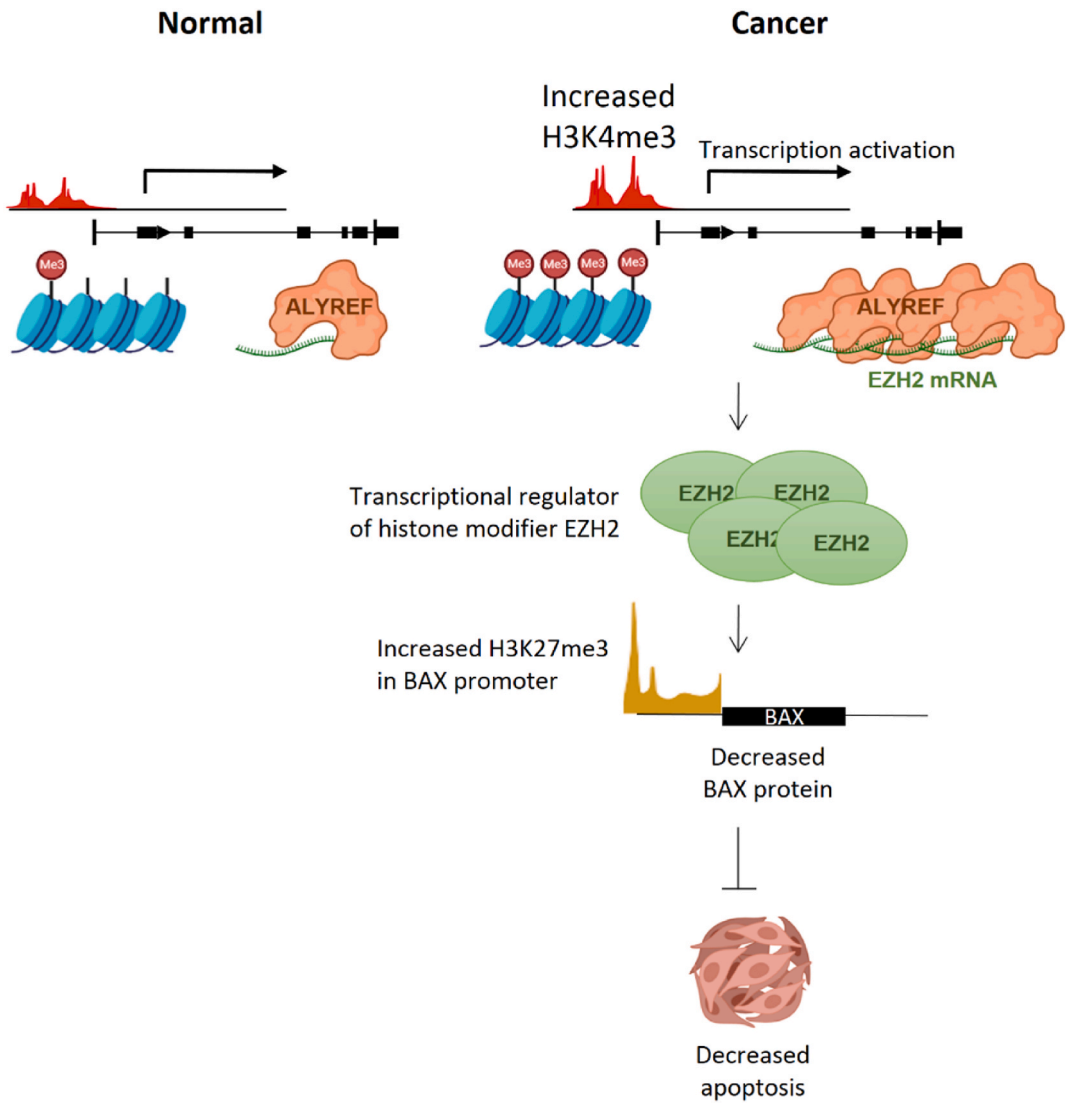

Fig. 6. Graphical abstract. Increased H3K4 trimethylation upregulates *ALYREF* transcription and translation. Enhanced *ALYREF* regulates EZH2 transcription and subsequent translation. In non-TNBC breast cancer cell lines, EZH2 is regulated at the transcriptional level by *ALYREF*, leading to increased H3K27me3 at the BAX promoter, followed by the repression of BAX mRNA and protein. Decreased BAX expression rendered non-TNBC cancer cells resistant to apoptosis.

4. Discussion

H3K4me3 is widely recognized as a hallmark of gene promoters. Intergenic H3K4me3 peaks have been suggested to potentially indicate unannotated promoters of protein-coding genes or lncRNAs in human studies [42,43]. Additionally, previous research indicates that H3K4me3 marks exon-intron boundaries and helps recruit general transcription factors to promoters [44]. In this study, genome-wide ChIP-seq analysis showed a high enrichment of H3K4me3 at the ALYREF promoter, and ALYREF expression levels were higher in CMT compared to normal tissues. *ALYREF* depletion decreased cell viability and colony formation assay, while increasing apoptosis in CMT and human breast cancer cells. Significantly higher levels of *ALYREF* mRNA and protein were observed in hormone receptor-positive cancer cell lines (MCF7 and SKBR3) than in normal breast cell lines. When comparing DNA and amino acid sequences, we found that the homology between canine and human *ALYREF* was more pronounced than that between mouse and canine and/or human *ALYREF*.

The dysregulation of RNA-binding proteins has been reported in various types of cancers [17–20]. ALYREF is one of the key molecules involved in RNA metabolism and the export of mRNAs, in combination with RNA helicase USP56 and THO complexes, from the nucleus to the cytosol [45]. The mRNA transport function of *ALYREF* is crucial for the proper translation of transported mRNAs and the function of their proteins. In this study, we showed that *ALYREF* can facilitate the oncogenic process by elevating the histone modifier EZH2 (H3K27me3 writer) and, in turn, upregulating anti-apoptotic genes such as *BAX*, as illustrated in Fig. 6.

In a TNBC cohort, *ALYREF* was reported to regulate the oncogenic lncRNA, lncNEAT1-1, through a distinct mechanism. First, it modulates transcription by binding to the NEAT1 promoter region. Secondly, it directly binds to and stabilizes lncNEAT 1-1 and CPSF6, which is an activator of NEAT1. In breast cancer, *ALYREF* copy number alteration (in an average of 5 % of breast cancer patients) is one of the regulatory mechanisms of ALYREF expression. According to the c-Bioportal database, *ALYREF* is upregulated in 5%–15 % of patients with breast cancer. In previous studies, the upregulation of *ALYREF* was revealed through copy number variation (CNV) in a TNBC cohort [20]. However, the oncogenic functions of *ALYREF* in hormone receptor-positive breast cancer and its underlying epigenetic mechanisms were poorly understood. In our study of hormone receptor-positive breast cancer, *ALYREF* was found to have oncogenic features.

ALYREF is upregulated in various cancers, including low-grade gliomas [19], HCC [17] and TNBC [20]. In neuroblastomas, ALYREF binds to MYCN, forming a transactivator complex that upregulates USP3, a deubiquitinating enzyme of MYCN. Because *ALYREF* is a *MYC* target gene, increased MYC protein stability leads to *ALYREF* expression [18]. In glioblastomas, *ALYREF* is regulated by MYC and promotes oncogenic pathways and tumor growth. *ALYREF* binds to and stabilizes *MYC* mRNAs, contributing to the carcinogenesis of GBM, and overexpression of MYC restores oncogenic properties in *ALYREF*-deficient GBM cells [19].

We examined the expression levels of *MYC* and related genes after *ALYREF* depletion in SKBR3 and MCF7 cell lines, but no significant differences were observed (data not shown) [46]. DNA microarray analysis showed that *MYC* expression does not significantly increase in the luminal and HER2-enriched subtypes [46]. These observations suggest that *ALYREF* may influence MYC; however, MYC-mediated tumorigenesis appears to be less significant in luminal-type and HER-2 (MCF7 and SKBR3) breast cancers with low *MYC* expression.

We also considered another mechanism by which *ALYREF* regulates apoptosis in non-TNBC cell lines. Based on our results, increased apoptosis appeared to be mediated by elevated *BAX* proapoptotic gene expression. Furthermore, exploration of the epigenetic mechanisms related to histone modifications that contribute to apoptosis resistance in breast cancer revealed the epigenetic regulation of *BAX* in breast cancer cell lines (MCF7 and MDA-MB-231). We observed that H3K27me3 levels in the *BAX* promoter were increased in breast cancer cells. This is supported by a previous study showing that the EZH2 (H3K27me3 writer)-selective inhibitor ZLD1039 induces *BAX* expression in MCF7 and MDA-MB-231 cells [47]. EZH2 overexpression is frequently observed in invasive and metastatic breast cancers and is associated with poor prognosis [48]. ALYREF also binds to *EZH2* mRNA [16]. *ALYREF* depletion results in reduced gene expression and protein levels of EZH2. Previous studies have shown that *ALYREF* increases the mRNA export as well as mRNA stability. Increased *EZH2* expression and translation may be mediated by *ALYREF* in a manner similar to that by which ALYREF enhances lncNETA1-1 expression. *EZH2* and *lncNEAT1-1* are overexpressed in breast cancer and function as oncogenic factors. ALYREF regulates oncogenic factors through various mechanisms, acting as a transcription factor and enhancing the stability of mRNA and proteins involved in tumorigenesis.

5. Conclusion

Our data suggest that *ALYREF* affects EZH2 mRNA expression leading to upregulation of EZH2 protein levels in cancer cells. Increased EZH2 expression results in heightened H3K27me3 modification of the BAX promoter, reduced BAX expression, and decreased apoptosis in hormone receptor-positive cancer cell lines (ER-positive and HER2 enriched). Although further investigation is necessary to delineate the role of *ALYREF* in the downregulation of EZH2 in TNBC and luminal B-type breast cancer, our study is the first to demonstrate that ALYREF maintains EZH2 mRNA and protein levels. Moreover, an in-depth analysis of comparative epigenomics between canine and human breast cancers suggests that ALYREF is involved in common breast tumorigenesis in both species.

Data availability

All raw data of high-throughput sequencing data for generated in this study have been deposited to the NCBI SRA database in BioProject number PRJNA765478.

Funding

This research was supported by grants from the Ministry of Science and ICT, the National Research Foundation of Korea (NRF) SRC program, and the Comparative Medicine Disease Research Center (CDRC) in Korea (2021R1A5A103315714).

CRediT authorship contribution statement

Su-Jin Jeong: Writing – original draft, Visualization, Validation, Methodology, Formal analysis, Data curation. **Ji Hoon Oh:** Writing – review & editing, Supervision. **Je-Yoel Cho:** Writing – review & editing, Supervision, Investigation, Funding acquisition, Conceptualization.

Declaration of generative AI and AI-assisted technologies in the writing process

During the preparation of this study, the author utilized ChatGPT to verify the grammatical accuracy of the English text. After using this tool, the author reviewed and edited the content as necessary and assumed full responsibility for the final manuscript.

Declaration of competing interest

All authors declare no conflicts of interest.

Acknowledgment

We thank Dr. Kang-Hoon Lee, GeneOne Life Science, Inc., Seoul, Republic of Korea, for insightful discussions, Keun Hong Son for providing part of the bioinformatics analysis, and M. Aldonza for helping in establishing the CMT primary cell line. We would like to thank Wan Hee Kim, College of Veterinary Medicine, Seoul National University, for providing us with well-controlled clinical specimens.

Appendix A. Supplementary data

Supplementary data to this article can be found online at https://doi.org/10.1016/j.heliyon.2024.e37749.

References

[1] K. Michailidou, et al., Genome-wide association analysis of more than 120,000 individuals identifies 15 new susceptibility loci for breast cancer, Nat. Genet. 47 (4) (2015) 373–380.
[2] S.R. Johnston, Enhancing endocrine therapy for hormone receptor–positive advanced breast cancer: cotargeting signaling pathways, J. Natl. Cancer Inst. 107 (10) (2015) djv212.
[3] C.L. Arteaga, et al., Treatment of HER2-positive breast cancer: current status and future perspectives, Nat. Rev. Clin. Oncol. 9 (1) (2012) 16–32.
[4] R. Schneider, Comparison of age, sex, and incidence rates in human and canine breast cancer, Cancer 26 (2) (1970) 419–426.
[5] K.-H. Lee, et al., Transcriptome signatures of canine mammary gland tumors and its comparison to human breast cancers, Cancers 10 (9) (2018) 317.
[6] K.-H. Lee, et al., Somatic mutation of PIK3CA (H1047R) is a common driver mutation hotspot in canine mammary tumors as well as human breast cancers, Cancers 11 (12) (2019) 2006.
[7] S.M. Abdelmegeed, S. Mohammed, Canine mammary tumors as a model for human disease, Oncol. Lett. 15 (6) (2018) 8195–8205.
[8] F.L. Queiroga, et al., Canine mammary tumours as a model to study human breast cancer: most recent findings, in vivo 25 (3) (2011) 455–465.
[9] A. Nam, et al., Alternative methylation of intron motifs is associated with cancer-related gene expression in both canine mammary tumor and human breast cancer, Clin. Epigenet. 12 (1) (2020) 1–15.
[10] J.J. Schabort, et al., Ank2 hypermethylation in canine mammary tumors and human breast cancer, Int. J. Mol. Sci. 21 (22) (2020) 8697.
[11] S.-J. Jeong, et al., Genome-wide methylation profiling in canine mammary tumor reveals miRNA candidates associated with human breast cancer, Cancers 11 (10) (2019) 1466.
[12] K.-H. Lee, et al., Methylation of LINE-1 in cell-free DNA serves as a liquid biopsy biomarker for human breast cancers and dog mammary tumors, Sci. Rep. 9 (1) (2019) 175.
[13] M. Vermeulen, et al., Selective anchoring of TFIID to nucleosomes by trimethylation of histone H3 lysine 4, Cell 131 (1) (2007) 58–69.
[14] L. Berger, et al., Expression of H3K4me3 and H3K9ac in breast cancer, J. Cancer Res. Clin. Oncol. 146 (2020) 2017–2027.
[15] A. Chase, N.C. Cross, Aberrations of EZH2 in cancer, Clin. Cancer Res. 17 (9) (2011) 2613–2618.
[16] M. Shi, et al., ALYREF mainly binds to the 5′ and the 3′ regions of the mRNA in vivo, Nucleic acids research 45 (16) (2017) 9640–9653.
[17] C. Xue, et al., ALYREF mediates RNA m5C modification to promote hepatocellular carcinoma progression, Signal Transduct. Targeted Ther. 8 (1) (2023) 130.
[18] Z. Nagy, et al., An ALYREF-MYCN coactivator complex drives neuroblastoma tumorigenesis through effects on USP3 and MYCN stability, Nat. Commun. 12 (1) (2021) 1881.
[19] J. Wang, et al., ALYREF drives cancer cell proliferation through an ALYREF-MYC positive feedback loop in glioblastoma, OncoTargets Ther. (2021) 145–155.
[20] C. Klec, et al., ALYREF, a novel factor involved in breast carcinogenesis, acts through transcriptional and post-transcriptional mechanisms selectively regulating the short NEAT1 isoform, Cell. Mol. Life Sci. 79 (7) (2022) 391.
[21] H.J. Hwang, K.H. Lee, J.Y. Cho, ABCA9, an ER cholesterol transporter, inhibits breast cancer cell proliferation via SREBP-2 signaling, Cancer Sci. 114 (4) (2023) 1451.
[22] R. Uyama, et al., Establishment of four pairs of canine mammary tumour cell lines derived from primary and metastatic origin and their E-cadherin expression, Vet. Comp. Oncol. 4 (2) (2006) 104–113.

[23] B.N.R. Lee, et al., IFN-γ enhances the wound healing effect of late EPC s (LEPC s) via BST 2-mediated adhesion to endothelial cells, FEBS Lett. 592 (10) (2018) 1705–1715.
[24] S.-A. Lee, et al., METTL8 mRNA methyltransferase enhances cancer cell migration via direct binding to ARID1A, Int. J. Mol. Sci. 22 (11) (2021) 5432.
[25] K.H. Son, et al., Integrative mapping of the dog epigenome: reference annotation for comparative intertissue and cross-species studies, Sci. Adv. 9 (27) (2023) eade3399.
[26] C. Peng, et al., Integrated analysis of differentially expressed genes and pathways in triple-negative breast cancer, Mol. Med. Rep. 15 (3) (2017) 1087–1094.
[27] A.C. Newman, O.D. Maddocks, One-carbon metabolism in cancer, Br. J. Cancer 116 (12) (2017) 1499–1504.
[28] N.I. Kim, et al., Squalene epoxidase expression is associated with breast tumor progression and with a poor prognosis in breast cancer, Oncol. Lett. 21 (4) (2021) 1.
[29] C. Chokchaitaweesuk, et al., Enhanced hexosamine metabolism drives metabolic and signaling networks involving hyaluronan production and O-GlcNAcylation to exacerbate breast cancer, Cell Death Dis. 10 (11) (2019) 803.
[30] M.J. Lewis, J.P. Wiebe, J.G. Heathcote, Expression of progesterone metabolizing enzyme genes (AKR1C1, AKR1C2, AKR1C3, SRD5A1, SRD5A2) is altered in human breast carcinoma, BMC Cancer 4 (2004) 1–12.
[31] S.Y. Jun, et al., Reduction of squalene epoxidase by cholesterol accumulation accelerates colorectal cancer progression and metastasis, Gastroenterology 160 (4) (2021) 1194–1207. e28.
[32] D.N. Brown, et al., Squalene epoxidase is a bona fide oncogene by amplification with clinical relevance in breast cancer, Sci. Rep. 6 (1) (2016) 19435.
[33] H. Lee, et al., Prognostic and therapeutic impact of a homologous recombination repair protein TONSL in cancer stem cells, Cancer Res. 83 (7_Supplement) (2023) 6104.
[34] A.S. Khatpe, et al., TONSL is an immortalizing oncogene and a therapeutic target in breast cancer, Cancer Res. 83 (8) (2023) 1345–1360.
[35] G. You, et al., COMMD proteins function and their regulating roles in tumors, Front. Oncol. 13 (2023) 1067234.
[36] C.G. Campion, et al., Does Subtelomeric position of COMMD5 influence Cancer progression? Front. Oncol. 11 (2021) 642130.
[37] L. Guo, et al., CCDC137 is a prognostic biomarker and correlates with immunosuppressive tumor microenvironment based on pan-cancer analysis, Front. Mol. Biosci. 8 (2021) 674863.
[38] W. Li, et al., P3H4 is correlated with clinicopathological features and prognosis in bladder cancer, World J. Surg. Oncol. 16 (2018) 1–6.
[39] T. Wang, et al., P3H4 regulates apoptosis and autophagy of breast cancer cells via BCL-2/BAX/Caspase-3 and AMPK/mTOR/ULK1 signaling pathways, Mol. Biol. (2024) 1–12.
[40] Y.-p. Zhang, et al., Over-expression of SRD5A3 and its prognostic significance in breast cancer, World J. Surg. Oncol. 19 (2021) 1–11.
[41] H. Widden, W.J. Placzek, The multiple mechanisms of MCL1 in the regulation of cell fate, Commun. Biol. 4 (1) (2021) 1029.
[42] T.S. Mikkelsen, et al., Genome-wide maps of chromatin state in pluripotent and lineage-committed cells, Nature 448 (7153) (2007) 553–560.
[43] M. Guttman, et al., Chromatin signature reveals over a thousand highly conserved large non-coding RNAs in mammals, Nature 458 (7235) (2009) 223–227.
[44] N.I. Bieberstein, et al., First exon length controls active chromatin signatures and transcription, Cell Rep. 2 (1) (2012) 62–68.
[45] T. Pühringer, et al., Structure of the human core transcription-export complex reveals a hub for multivalent interactions, Elife 9 (2020) e61503.
[46] J. Xu, Y. Chen, O.I. Olopade, MYC and breast cancer, Genes & cancer 1 (6) (2010) 629–640.
[47] X. Song, et al., Selective inhibition of EZH2 by ZLD1039 blocks H3K27methylation and leads to potent anti-tumor activity in breast cancer, Sci. Rep. 6 (1) (2016) 20864.
[48] C.G. Kleer, et al., EZH2 is a marker of aggressive breast cancer and promotes neoplastic transformation of breast epithelial cells, Proc. Natl. Acad. Sci. USA 100 (20) (2003) 11606–11611.